Biodegradable Synthetic Organelles Demonstrate ROS Shielding in Human-Complex-I-Deficient Fibroblasts

Lisanne M. P. E. van Oppen,[†,‖,#] Loai K. E. A. Abdelmohsen,[‡,#] Sjenet E. van Emst-de Vries,[†] Pascal L. W. Welzen,[‡] Daniela A. Wilson,[§] Jan A. M. Smeitink,[‖] Werner J. H. Koopman,[†] Roland Brock,[†] Peter H. G. M. Willems,*[,†] David S. Williams,*[,⊥] and Jan C.M. van Hest*[,‡]

[†]Department of Biochemistry, Radboud Institute for Molecular Life Sciences (RIMLS), Radboud University Medical Center, PO Box 9101, 6500 HB Nijmegen, The Netherlands

[‡]Department of Biomedical Engineering & Department of Chemical Engineering and Chemistry, Eindhoven University of Technology, PO Box 513, 5600 MB Eindhoven, The Netherlands

[§]Institute for Molecules and Materials (IMM), Radboud University, Heyendaalseweg 135, 6525 AJ Nijmegen, The Netherlands

[‖]Department of Pediatrics, Radboud Centre for Mitochondrial Disease, Radboud University Medical Center, Geert Grooteplein 10, PO Box 9101, 6500 HB Nijmegen, The Netherlands

[⊥]Department of Chemistry, Swansea University, SA2 8PP Swansea, United Kingdom

S *Supporting Information*

ABSTRACT: Biodegradable, semipermeable nanoreactors that are capable of undergoing cellular integration and, subsequently, function as synthetic organelles represent an exciting therapeutic technology. Polymersomal nanoreactors have been investigated as a suitable candidate for the engineering of such a system, with the chemical versatility and structural robustness required for such a demanding application. Although steps have been taken to demonstrate this capacity, there has yet to be a system presented with biochemically robust data showing therapeutic efficacy in primary human cells. The reason for this shortfall is the absence of essential criteria of the polymersomes tested so far; biodegradability, intrinsic semipermeability, and a biomedically relevant setting. Herein, we present enzyme-loaded, biodegradable poly(ethylene glycol)-*block*-poly(caprolactone-*gradient*-trimethylene carbonate) (PEG−PCLgTMC) polymersomal nanoreactors, readily fabricated using the biocompatible direct hydration methodology. Physical characterization of PEG−PCLgTMC polymersomes highlights their semipermeable membrane and ability to shield enzymatic cargo. Surface modification with cell-penetrating peptides (CPPs) directs cellular integration of enzyme-loaded PEG−PCLgTMC nanoreactors in a controlled fashion. Using HEK293T cells and human skin fibroblasts we demonstrate that biocompatible catalase nanoreactors successfully perform as a synthetic organelle, imparting activity-dependent antioxidant (reactive-oxygen-species-shielding, ROS-shielding) capacity to cells. Notably, for the first time, patient-derived human-complex-I-deficient primary fibroblasts are effectively protected against the toxicity of exogenous H_2O_2 by the action of internalized enzyme-loaded nanoreactors, showcasing this system in a therapeutically relevant context.
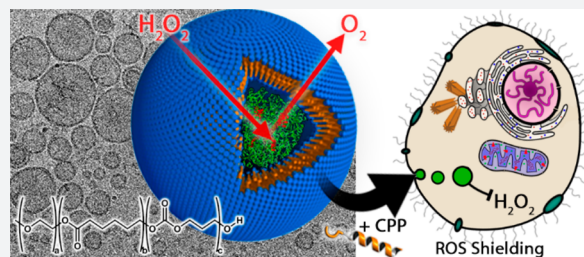
INTRODUCTION

Membrane-bound organelles (such as mitochondria, endosomes, or the nucleus) are compartmentalized microenvironments where diverse enzymatic processes take place under highly regulated conditions.[1,2] A striking feature of such subcellular compartments is that they permit selective transmembrane molecular transport, a property vital for their function. The physicochemical elegance of organelles has inspired scientists to engineer synthetic counterparts, capable of performing complex function within the cell.[2−5] Indeed, substantial progress has been made in this area through the utilization of both micro- and nanocompartments.[6,7] Notable developments toward the *in vitro* application of microreactors (based on polymer capsules or liposomes) have been presented, with uptake into macrophages facilitated by macropinocytosis or via a microinjection method for other cell types.[8−10] Although there are undoubtable advantages in using larger, more structurally complex microreactors, their large size makes them less versatile as compared to their nanoscopic counterparts. In particular, copolymer vesicles (polymersomes), synthetic replicas of liposomes, which are capable of encapsulating and stabilizing sensitive internal cargo (such as enzymes),[7,11] have great potential for cellular therapy.[12,13] In particular, their utility as organelle-like nanosystems, capable of endogenously affecting cellular chemistry and performing tasks that would otherwise be malfunctioning (or absent), is an exciting prospect. Nano-

reactors, based on polymersomal (and polymer capsule) technology, have been shown to undergo cellular integration, and confined enzyme activity was demonstrated with a number of cell lines *in vitro*.[14−19] Moreover, pioneering studies using nanoreactors *in vivo* have yielded interesting results, with superoxide-dismutase-loaded polymersomes functioning as antioxidants to reduce neuropathic pain (rat model) and β-galactosidase-loaded polyion complex vesicles (PICsomes) showing specific function within tumor tissue (mouse model).[20,21]

Evaluation of recent studies highlights essential properties that are of critical importance for the effective functioning of synthetic organelles: semipermeability, biodegradability, and biocompatibility. Regarding the former, progress has been made with both membrane postmodification (channel proteins, DNA pores, or chemically),[22−31] and complex morphological engineering,[32,33] to generate functioning nano-reactors. Engineering polymersomal nanoreactors with an intrinsically semipermeable membrane remains a challenge, however, with few examples that are sufficiently permeable to facilitate native chemical processing of external substrates utilizing compartmentalized enzyme(s).[34−40] Even more challenging is to realize such a system that is both biodegradable and biocompatible, vital features of a synthetic organelle to ensure cellular integration without toxic side effects that would undermine biomedical application. To this end, we have undertaken to engineer, via the remarkably facile direct hydration approach, a biodegradable, semipermeable polymersomal platform that can function as autonomous nanoreactors through enzyme encapsulation. Recently, we presented the direct hydration method for preparation of poly(ethylene glycol)−poly(caprolactone) (PEG−PCL) poly-mersomes, using oligo(ethylene glycol) (OEG) as a nontoxic dispersant.[41] This methodology can facilitate biomolecular encapsulation;[42] however, it has not yet been presented as a route toward nanoreactor fabrication.

Although the design and fabrication of biodegradable (autonomous) nanoreactors are already a substantial challenge, it is important to apply them toward a quantitative biochemical evaluation using an appropriate therapeutic target that will take us beyond proof-of-principle. In this respect, the pathological effect of hydrogen peroxide (H_2O_2) is a medically relevant topic of investigation. H_2O_2 is highly diffusible and relatively long-lived,[43] serving as a key molecule in redox signaling, control, and regulation.[44] Mitochondria are an important source of intracellular reactive oxygen species (ROS), resulting from superoxide dismutation into H_2O_2 at complexes I (CI) and III (CIII), which is subsequently oxidized (into water) by cytosolic and mitochondrial peroxidases as well as peroxisomal catalase. When the native antioxidant capacity is overwhelmed by ROS,[45] oxidative stress in cells occurs, which is implicated in the pathogenesis of many disorders such as Alzheimer's, Parkinson's, Huntington's, and metabolic diseases alongside aging and cancer, more generally.[46−48] Therefore, the generation of antioxidant nanoreactors (AONs), which can be spontaneously integrated into cells that are experiencing heightened-ROS levels, is a strategy that has great medical potential. Indeed, acatalasemia, an autosomal recessive condition that results in a >90% reduction in cellular catalase activity, is an example where such a strategy could be highly effective. Individuals with inherited catalase deficiency have a high prevalence of diabetes mellitus (18.5%) and of diseases related to oxidative stress (85%).[49] In mice models, studies show that catalase deficiency leads to ROS sensitivity,[50] whereas catalase overexpression prolongs lifespan and attenuation of age-related pathologies.[51−53] Mitochondrial CI deficiency is associated with neurodegeneration, and studies using primary (patient-derived) skin fibroblasts indicate an imbalance between the production and scavenging of ROS.[54,55] Studies on mice with malfunctioning CI also indicated that increases in neuronal ROS are an important part of the neurodegeneration process.[56] Therefore, with increased attention being paid to the development of advanced therapeutic technologies to tackle age- and cancer-related diseases, attenuation of (cellular) ROS stress is an excellent niche to focus on.

Herein, we present for the first time catalase-loaded, semipermeable polymersomes (comprising biodegradable copolymers) as antioxidant nanoreactors (AONs) in a medically relevant application. We demonstrate (and quantify) the capacity of AONs to function as synthetic organelles, providing effective shielding of patient-derived primary cells from ROS *in vitro* (Figure 1). Such unprecedented application
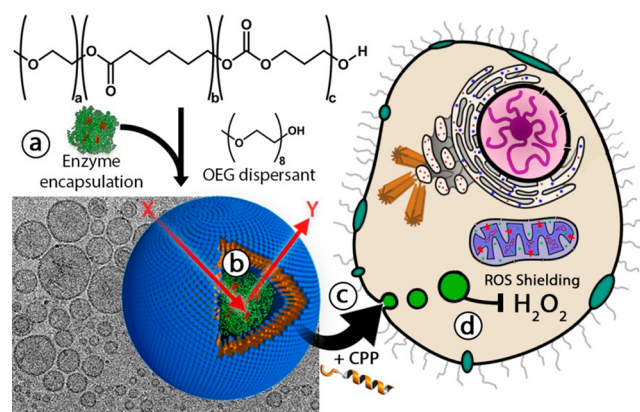

Figure 1. Engineering a biodegradable synthetic organelle. (a) Poly(ethylene glycol)-*block*-poly(caprolactone-*gradient*-trimethylene carbonate) (PEG−PCl*g*TMC) copolymers were synthesized and, utilizing the direct hydration method, underwent controlled self-assembly into polymersomes that could be loaded with enzymatic cargo. (b) PEG−PCl*g*TMC polymersomes that possess a semi-permeable membrane facilitate transmembrane substrate diffusion for compartmentalized enzymatic reactions (e.g., X = D-glucose and Y = gluconolactone/H_2O_2), functioning as autonomous nanoreactors. (c) Cellular integration is directed by attaching a cell-penetrating peptide (CPP) to the polymersome surface. (d) Antioxidant polymersomes (containing catalase) demonstrate ROS shielding in both HEK 293 and (primary) human fibroblasts.

of this technology makes the important step from proof-of-principle research to a biomedically relevant platform, which reflects the robustness and versatility of this approach and will, hopefully, inspire further development toward realization of synthetic organelles in clinical studies.

■ RESULTS AND DISCUSSION

Engineering Biodegradable PEG−PCL*g*TMC Polymer-somes via Direct Hydration. The essential requirements for polymersomal nanoreactors to be successfully implemented as synthetic organelles are biocompatibility and semipermeability. To accomplish this goal we set out to develop biodegradable block copolymers (BCPs) in order to generate self-assembled nanostructures with the desired properties.[57] BCPs comprising
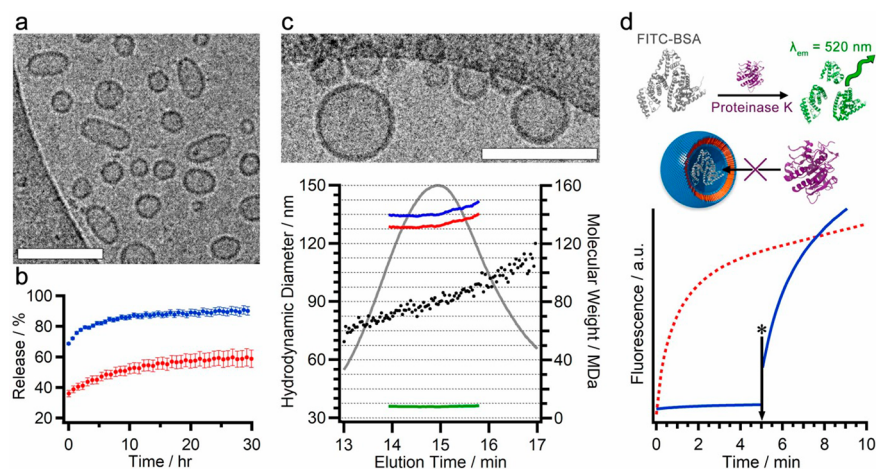
Figure 2. Characterization of semipermeable PEG−PCLgTMC polymersomes. (a) Cryo-TEM image of mPEG$_{22}$-50/13 (50 wt % TMC in hydrophobic block/13 wt % overall hydrophilic PEG content) polymersomes, fabricated by direct hydration from a 10 wt % OEG solution. (b) Calcein release curves for mPEG$_{22}$-50/13 (red) and mPEG$_{12}$-50/13 (blue) polymersomes. (c) Characterization of eGFP-loaded polymersomes using cryo-TEM (upper) and AF4-MALS/DLS (lower)—molecular weight of copolymer (red) and eGFP (green) in polymersomes (total mass in blue) was calculated from the corresponding dn/dc values and plotted against size (spheres) with the scattering fractogram inserted for reference (gray). (d) Macromolecular shielding of encapsulated FITC−BSA substrate from proteinase K degradation (blue line) as compared to the free substrate (red dashes). Polymersome disruption by surfactant addition (*) caused content leakage and rapid degradation of internal cargo. All scale bars = 200 nm.

poly(ethylene glycol) (PEG) with various hydrophobic, biodegradable polymers such as poly(caprolactone) (PCL), poly(lactide) (PLA), or poly(trimethylene carbonate) (PTMC) have been presented as biocompatible building blocks for the preparation of polymersomes.[58−65] Recently, we reported the self-assembly of PEG−PCL via an unconventional direct hydration process,[42] replacing harmful solvents with nontoxic low molecular weight oligo(ethylene glycol) (OEG).[41] Although PCL is a commonly used polyester in biomedical research,[66] its high T_c (ca. 55−60 °C) impedes control over self-assembly and causes undesirable membrane properties. Therefore, if we are to use BCPs related to PCL in the self-assembly of polymersomal nanoreactors, crystallinity should be reduced. To achieve this, it has been reported that copolymerization of caprolactone with a distinct monomer (capable of reducing overall crystallinity) imparts greater control over self-assembly.[60]

Inspired by this work, we adopted a strategy for the preparation of (noncrystalline) gradient copolymers comprising PCL and poly(trimethylene carbonate) (PCLgTMC) via organocatalyzed ring-opening polymerization.[67,68] Using monomethoxy-PEG polymers as macroinitiator, we produced a series of well-defined block copolymers (Đ ≤ 1.1) of PEG−PCLgTMC using methanesulfonic acid as a nontoxic catalyst (Figure S1a and Table S1). As both chemical and physical factors affect BCP self-assembly, optimization of both copolymer composition and their direct hydration was performed. For chemical optimization, PEG−PCLgTMC BCPs with varying PEG length (X), TMC content in the hydrophobic block (Y, wt %), and overall hydrophilic content (Z, wt %) were prepared, designated mPEG$_X$-Y/Z. It was determined that a TMC content of at least 20 wt % was sufficient to suppress PCL crystallinity (Figure S2). Cryo-TEM screening indicated that the optimal composition for polymersome formation was close to mPEG$_{12}$ or mPEG$_{22}$-50/13 with longer chains based on mPEG$_{42}$ forming clustered spheroids (Figure 2a and Figure S3a−c). Either increasing or decreasing the TMC content led to coformation of spherical or wormlike

micelles, respectively, and increasing the overall hydrophilic content led to poorly defined morphologies (Figure S3d−f). Physical optimization of direct hydration involved maximizing the [copolymer] in OEG (prior to hydration) and minimizing the amount of buffer necessary to induce subsequent polymersome formation, so as to make protein encapsulation more favorable (process outlined in Figure S1). While [copolymer] (in OEG) > 10 wt % resulted in visible aggregation, formulation at 10 wt % resulted in uniform polymersomes and was, therefore, chosen for further tests. Using a combination of asymmetric flow field-flow fractionation (AF4) coupled with dynamic light scattering (AF4-DLS) we confirmed that adding 80 μL of phosphate-buffered saline (PBS) in the hydration of 20 μL of (stirred) OEG/copolymer solution (mPEG$_{22}$-50/13) was optimal to obtain polymersomes of ca. 100 nm in size (Figure S4). After stirring the cloudy solution for 5 min, subsequent dilution with 400 μL of PBS yielded a visually homogeneous polymersome suspension with [copolymer] = 4 mg/mL.

Analysis of polymersomes comprising mPEG$_{12}$/mPEG$_{22}$-50/13 (by AF4-DLS) yielded average sizes of 200 and 100 nm, respectively (Figure S5a). Analysis of membrane thickness from cryo-TEM images yielded values of around 7 and 14 nm, respectively (Figure S5b). To confirm whether OEG is truly a dispersant in the direct hydration process, or if it interacts to some extent with the polymersomal membrane, nuclear Overhauser spectroscopy (NOESY) was performed, to assess the degree of spatial correlation between membrane protons and those of OEG. It was observed that the sharp OEG peak at 3.75 ppm was distinct from the broad coronal PEG peak at 3.72 ppm (Figure S6). We were therefore confident that OEG only functioned as a dispersant and had no structural role.

Semipermeability, Protein Encapsulation, and Shielding Properties of Polymersomes. With a platform for the facile preparation of well-defined, biodegradable polymersomes, a calcein release assay was performed to probe the permeability of the PCLgTMC membrane. Monitoring calcein release by the dequenching of its
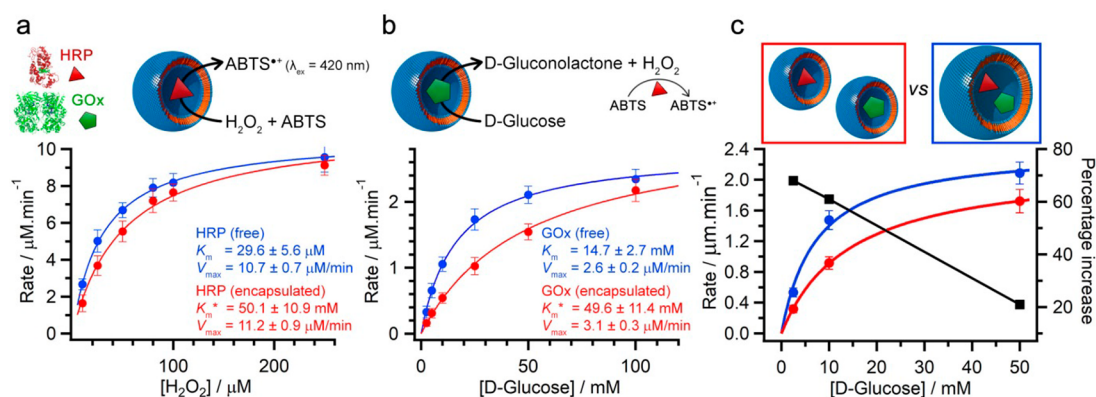
Figure 3. Nanoreactor characterization of enzyme-loaded polymersomes using Michaelis−Menten kinetic plots to compare free and encapsulated (a) HRP and (b) GOx alongside (c) a mono- (red) and coencapsulated (blue) HRP/GOx cascade; the black curve shows the difference in rate between the co- and monoencapsulated systems.

fluorescence signal, it was evident that both $mPEG_{12}$ and $mPEG_{22}$-50/13 polymersomes were semipermeable. $mPEG_{12}$-50/13 polymersomes showed a faster release profile with ca. 90% of encapsulated dye released after 30 h as compared to ca. 60% in the case of the thicker-walled, $mPEG_{22}$-50/13 counterpart (Figure 2b). Degradation studies, where polymersomes were diluted into human serum, revealed a striking difference between the stability of polymersomes comprising $mPEG_{12}$ and $mPEG_{22}$ copolymers. Although both scattering and DLS confirmed that $mPEG_{22}$-50/13 polymersomes did not show any degradation within 24 h, $mPEG_{12}$-50/13 degraded rapidly within 3 h (Figure S7). This observed behavior was attributed to the thinner membrane of $mPEG_{12}$-50/13 polymersomes and contributed to our decision to use $mPEG_{22}$-50/13 as the basis for our studies. The observed semipermeability and biodegradability of soft PEG−PCL*g*TMC polymersomes make them an exciting candidate for development as autonomous (not requiring any additional modification) nanoreactors.

To evaluate protein loading in this system we encapsulated eGFP (5 mg/mL) and employed AF4 coupled with multiangle light scattering (AF4-MALS) to quantitate loading and give an indication of efficiency using this method (optimized for polymersome stability). Size exclusion chromatograms indicated, as expected, that a large population of unencapsulated eGFP exists in solution, which could be recollected if desired and reused in a scale-up process (Figure S8a). AF4 fractograms of eGFP-loaded polymersomes demonstrated the capacity for protein loading in this system, with a clear signal at 480 nm and a substantial reduction in the radius of gyration of the polymersomes, both indicative of cargo loading (Figure S8b,c). Having measured the refractive index increment (d*n*/d*c*) of PEG−PCL*g*TMC (0.078), the extinction coefficient of eGFP (ε_{480} = 55 000 M^{-1} cm^{-1}) was used to quantitate polymersome loading. By mass, the eGFP content averaged around 5 wt %, equivalent to approximately 200 proteins per polymersome with an approximate [eGFP]$_{internal}$ in the region 20−60 mg/mL (Figure 2c). A fundamental property of compartmentalized systems is that they are capable of shielding sensitive cargo from degradation. By encapsulating a self-quenching FITC−BSA substrate we were able to demonstrate this property in the PEG−PCL*g*TMC polymersomes. While the polymersome remained intact, proteinase K was not able to permeate the membrane, until concentrated surfactant was added into the

system that resulted in rupture and rapid degradation of the sensitive cargo (Figure 2d).

Enzyme-Loaded Polymersomes Function as Autonomous Nanoreactors. Through encapsulation of functional enzymatic cargo, such as glucose oxidase (GOx) and horseradish peroxidase (HRP), we evaluated the performance of PEG−PCL*g*TMC polymersomes as autonomous nanoreactors. Inductively coupled plasma mass spectrometry (ICPMS) was used to calculate the loading efficiencies of ruthenium-labeled GOx and HRP, which were 4.2% (±0.2) and 1.2% (±0.3), respectively. Although HRP was appreciably lower than GOx this reflects known (but poorly understood) variations in encapsulation efficiencies between different enzymes.[37,38] Encapsulation efficiency values vary to the former value presented for eGFP due to the nature of the measurement; i.e., the latter was a direct content measurement in purified polymersomes. Subsequent assays were designed to compare the kinetics of free and encapsulated enzymes. Because exact [enzyme] encapsulated could not be determined to the necessary degree of accuracy, only the Michaelis constant (K_M) was evaluated.

First, the kinetics of either HRP- or GOx-loaded nanoreactors was evaluated using ABTS peroxidation as a photometric readout (Figure 3a,b). Either H_2O_2 or D-glucose were used as substrates for assays using HRP or GOx, respectively, with HRP used in excess for the latter and ABTS always used at a saturating concentration. Interestingly, increases in the observed K_M values (K_M(obs)) were measured for both encapsulated systems, with ca. 70% increase for HRP and ca. 240% increase for GOx. Although V_{max} values were similar, the apparent increase in K_M(obs) is striking and can be best understood by the diffusive barrier experienced by encapsulated enzyme arising from the semipermeable (PCL*g*TMC) membrane. In the case of HRP this arises due to the hampered diffusion of H_2O_2 into the nanoreactor (reducing the actual [substrate] at the enzyme), and for GOx this arises due to the hampered diffusion of glucose in *and* H_2O_2 out of the compartment. It is therefore consistent that K_M(obs) values for GOx are almost 4-fold larger, as compared to HRP. To demonstrate the positive benefits of compartmentalization, experiments were performed to compare the consequences of coencapsulation on the performance of the cascade reaction. In accordance with the previous data, a kinetic improvement in the cascade was observed in the coencapsulated system as compared to the mixture of
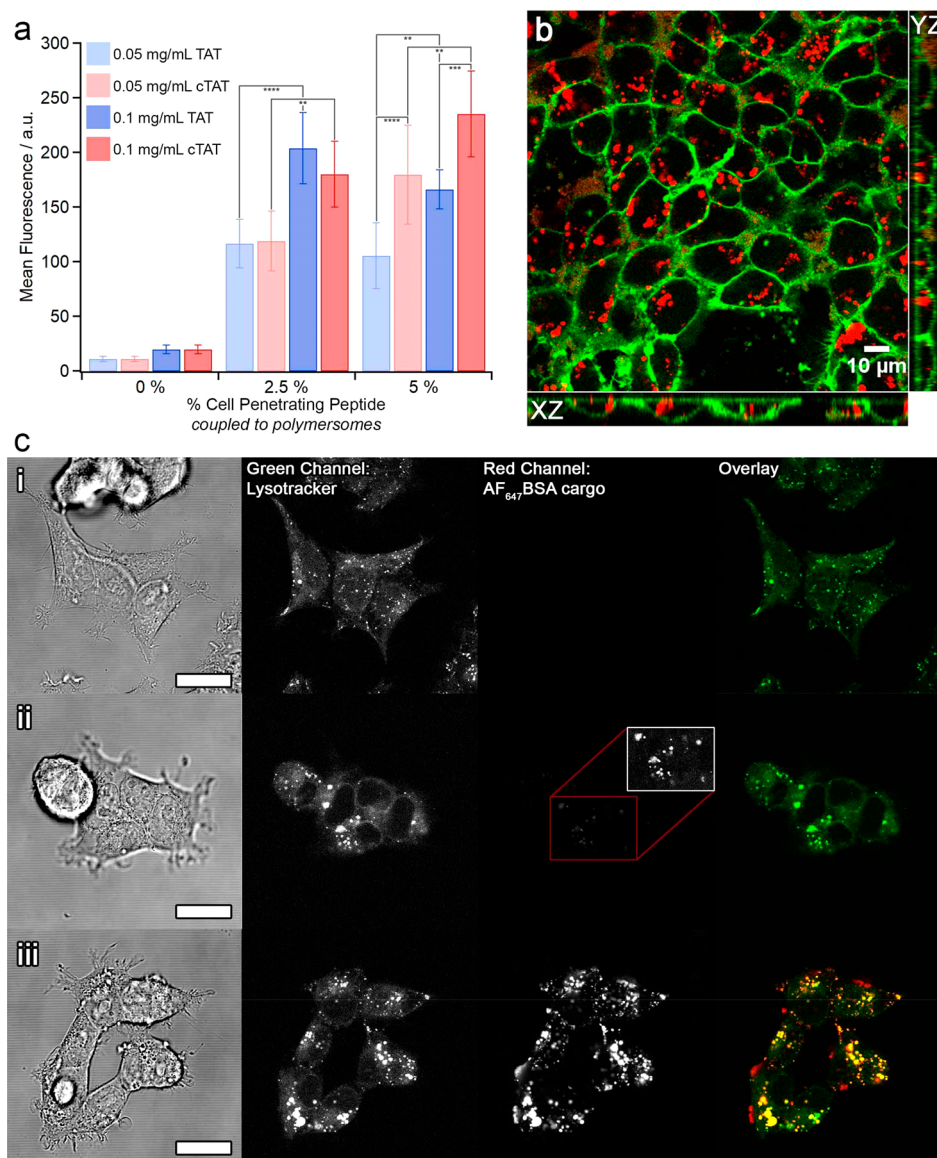
Figure 4. Cell uptake of cTAT polymersomes in HEK293T cells. (a) Uptake of NBD-labeled polymersomes after 24 h at different polymersome concentrations (0.05−0.1 mg/mL) and with different percentages of CPP (0−5%), quantified by flow cytometry (mean fluorescence of live cells presented ± SD, $n = 3$). Significant differences are indicated by $**P < 0.01$, $***P < 0.001$, $****P < 0.0001$. (b) Confocal microscopy images (sequential excitation mode) depicting the subcellular distribution of 2.5% TAT-polymersomes encapsulating $AF_{647}BSA$ (red) after 24 h of incubation at a concentration of 0.4 mg/mL (plasma membrane stained with CellMask green). (c) Confocal microscopy images (simultaneous excitation mode) depicting the endolysosomal localization of 2.5% TAT-polymersomes encapsulating $AF_{647}BSA$ after a 1 h pulse with 0.4 mg/mL polymersomes followed by a 24 h chase period in polymersome-free medium (acidic cellular compartments stained with LysoTracker green): (i) LysoTracker green, (ii) LysoTracker green and free $AF_{647}BSA$, (iii) LysoTracker green and 2.5% TAT-polymersomes encapsulating $AF_{647}BSA$. For visualization purposes, bright-field images were contrast-optimized using a linear contrast stretch (LCS) operation. Scale bars = 10 μm.

monoencapsulated nanoreactors (Figure 3c). The observed percentage increase in the rate of ABTS peroxidation between mono- and coencapsulated nanoreactors decreased as [glucose] increased (from 70% to 20%). This observation was understood to arise from a more detrimental effect of substrate diffusion at lower [glucose], diminishing as saturating conditions are approached. Although our discussion has focused upon K_M and substrate diffusion, kinetic enhancements that arise due to compartmentalization cannot be discounted;[69] however, a full examination of this is beyond the scope of the present experimental work.

Cell Uptake of CPP-Functionalized Polymersomes. An effective strategy for inducing the cell uptake of polymersomal

nanoreactors is through surface decoration with cell-penetrating peptides (CPPs).[70,71] TAT, a CPP derived from human immunodeficiency virus (HIV),[72] is known to translocate the cell plasma membrane,[73] and direct endocytotic uptake of colloidal or proteinaceous cargo.[74] Having previously reported the successful cellular integration of TAT-polymersomes,[15] we wanted to evaluate whether more advanced properties of CPPs could be realized in this platform, such as endosomal escape.[75] Recently, the cyclic variant of TAT (cTAT) was reported to direct cytosolic delivery of proteins in HeLa cells, thereby bypassing the endolysosomal system.[76] Therefore, we decided to compare the efficacy of the linear and cyclic TAT variants in facilitating polymersomal uptake. Because the diverse morpho-
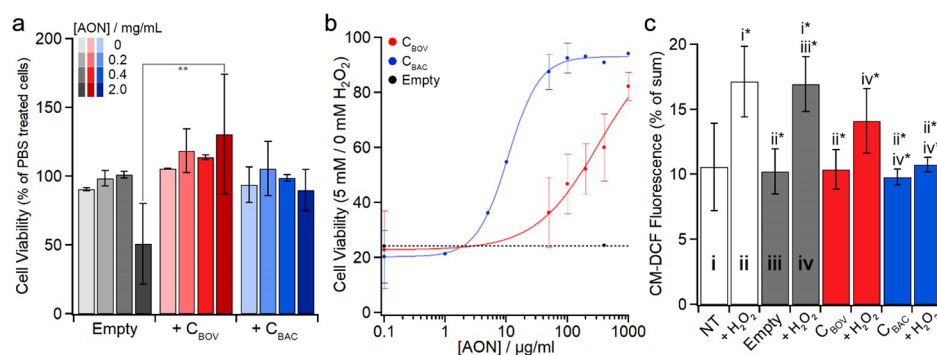
Figure 5. Functional analysis of antioxidant nanoreactors (AONs) in HEK293T cells. (a) Cytotoxicity of empty or C_{BOV}- or C_{BAC}-loaded AONs (after 24 h of incubation at concentrations of 0−2.0 mg/mL) was assessed by crystal violet absorbance measurements (mean ± SD, $n = 2$). (b) Dose-dependence protection of cells against H_2O_2-induced cell stress by AONs. Cells were pulse-treated with AONs for 1 h prior to a challenge with or without 5 mM of exogenous H_2O_2 for 24 h. Data presented as ratio of crystal violet signal obtained with 5 mM H_2O_2 to that without (where $n \geq 3$, mean ± SD, otherwise just the mean value is presented). (c) Effect of unloaded and C_{BOV} and C_{BAC} AONs on intracellular ROS assessed by CM-DCF fluorescence intensity measurements. Cells were treated with 0.4 mg/mL polymersomes for 24 h prior to loading with CM-H_2DCF and subsequent challenging with or without 0.5 mM of exogenous H_2O_2 for 5 min. Analysis was performed by flow cytometry with at least 10 000 cells per measurement. Data are presented as mean ± SD of 3 individual experiments after intraexperimental normalization to the sum of the values obtained. In panel c, significance was assessed using one-way ANOVA, followed by Tukey's multiple comparisons test. Significant differences are indicated by *$P < 0.05$, **$P < 0.01$.

logical features of nanoparticles (e.g., size, shape, stiffness, and surface topology) can significantly impact cellular uptake it is important to evaluate this key behavior in such a new system.[77,78] Cellular uptake and trafficking of polymersomes were evaluated in HEK293T cells after covalently coupling azido-TAT or azido-cTAT to fluorescent nitrobenzoxadiazole-doped (NBD-doped) polymersomes comprising either a 2.5 or 5 wt % doping of dibenzocyclooctyl-modified (DBCO-modified) PEG−PCLgTMC using biorthogonal click chemistry (Figure S9).

HEK293T cells were treated with polymersomes for 24 h prior to analysis of cell uptake by flow cytometry and confocal laser scanning microscopy (CLSM). Flow cytometry revealed that cell uptake was virtually absent for unmodified polymersomes (0% CPP), whereas TAT- and cTAT-polymersomes were readily taken up in a concentration-dependent manner (Figure 4a). At both concentrations, the effect of TAT was already maximal at 2.5% surface loading, whereas for cTAT a further increase was observed at 5%, suggesting the possibility of higher uptake with the latter TAT variant. In agreement with the flow cytometry data, CLSM showed virtually no cell uptake for unmodified polymersomes (Figure S10b). In sharp contrast, cTAT-polymersomes were abundantly present both at the cell membrane and within intracellular punctate structures (Figure S10c−f). Calculation of the Pearson's colocalization coefficient (PCC), which provides an estimate on the extent of overlap between green (polymersomes) and red (plasma membrane) pixels, showed no difference between TAT and cTAT for the two percentages tested (Figure S11). Similarly, the PCC did not differ between 2.5% and 5% TAT, whereas a significantly higher PCC value was observed at 5% cTAT. Because the data obtained did not show any beneficial effect of the cyclic variant, and due to its reduced tendency to accumulate in the cell membrane, TAT was used at its optimal concentration of 2.5% in further experiments. The ability of 2.5% TAT-polymersomes to deliver macromolecular cargo was demonstrated using Alexa647-labeled bovine serum albumin ($AF_{647}BSA$). Orthogonal projections of HEK293T cells treated with $AF_{647}BSA$-loaded polymersomes for 24 h unequivocally demonstrated the presence of cargo (red) in punctate

structures located within the cell (Figure 4b). Such structures are indicative of endolysosomal uptake, which was confirmed by pulse incubating cells with $AF_{647}BSA$ encapsulating 2.5% TAT-polymersomes for 1 h followed by a chase incubation of 24 h and staining with LysoTracker green showing a strong colocalization (PCC value of 0.6 ± 0.19; Figure S12). The possibility of cross-talk was excluded (Figure S13). Visual inspection of the Lyso Tracker green-positive structures (Figure 4c, second vertical row) shows a marked enlargement upon treatment with $AF_{647}BSA$ encapsulating 2.5% TAT-polymersomes. The overlay shows that these structures are $AF_{647}BSA$-positive, indicating the lysosomal accumulation of $AF_{647}BSA$-polymersomes. Similarly enlarged Lyso Tracker green-positive structures were observed upon treatment with free $AF_{647}BSA$ (Figure 4c, second vertical row). Also in this case these structures appeared, though extremely faintly, $AF_{647}BSA$-positive (Figure 4c, third vertical row). Because equal amounts of $AF_{647}BSA$ were used, either free or encapsulated, this result clearly demonstrates the strong uptake-facilitating properties of TAT-polymersomes. The 2.5% TAT-polymersomes, loaded with catalase, were used to add functionality to the cells in subsequent studies.

ROS Shielding by Catalase-Encapsulating TAT-polymersomes in HEK293T Cells. Having optimized the conditions for cellular uptake of TAT-functionalized polymersomes, the next step was to evaluate their function *in vitro* as a kind of "synthetic organelle". Through encapsulation of catalase, which is an important enzyme in protecting cells from oxidative damage, biological functionality was bestowed upon the TAT-polymersomes, to generate an antioxidant nanoreactor (AON). As CLSM clearly showed the predominant presence of TAT-polymersomes within the endolysosomal system, it is important to consider the function of such AONs at pH values ranging down to ∼5. With this in mind, we chose to compare two isoforms of catalase, from bovine (C_{BOV}) and bacterial (C_{BAC}) sources, with the latter being more stable at lower pH values. Functional comparison between AONs, which had a catalase encapsulation efficiency of 3.8% (±0.4), demonstrated that those fabricated with C_{BAC} were at least 8-fold more active than those encapsulating C_{BOV},
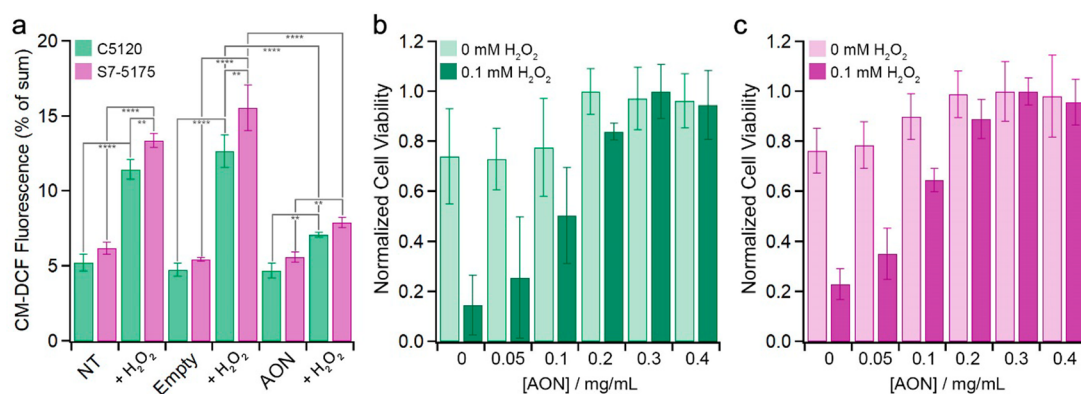
Figure 6. Functional analysis of AONs using primary skin fibroblasts from a healthy individual (C5120) and a patient with isolated complex I deficiency (S7-5175). (a) Intracellular ROS assessed by CM-DCF fluorescence intensity measurements after treatment with 0.4 mg/mL polymersomes for 24 h prior to challenge with or without 0.5 mM H_2O_2 for 5 min. Data are presented as mean $\pm$ SD of 3 individual experiments after intraexperimental normalization to the sum of the values obtained. Significance was assessed using two-way ANOVA, followed by Bonferroni's multiple comparisons test. Significant differences are indicated by $**P < 0.01$, $****P < 0.0001$. (b, c) Effect of C_{BAC}-AONs on cell integrity of (b) C5120 and (c) S7-5175 cells after a 1 h pulse treatment with a range of AON concentrations, followed by a 4 h chase period and a subsequent 24 h challenge with or without 0.1 mM H_2O_2. Data are presented as mean $\pm$ SD from 2 experiments performed in duplicate after intraexperimental normalization to the sum of the values obtained.

at all pH values measured (Figure S14). This difference in activity is most probably accounted for by a difference in intrinsic activity per unit enzyme. In accordance with the decreased sensitivity to pH, at pH 4.5 the C_{BAC} polymersomes were more active by a factor of 19-fold (Figure S14b). DLS and cryo-TEM were used to confirm the stability of AONs after catalase encapsulation, surface modification with 2.5% TAT, and purification (Figure S15). It was also confirmed that addition of H_2O_2 (5 mM) did not disrupt AON morphology as no change in scattering behavior was observed (Figure S15b).

To address the functionality of the AONs as synthetic organelles we assessed their capability to shield HEK293T cells against the detrimental effects of exogenous H_2O_2. Cell integrity analysis (using crystal violet) showed that empty 2.5% TAT-polymersomes were not cytotoxic when used for 24 h at a concentration up to 0.4 mg/mL (Figure 5a). However, a reduction in cell integrity was observed at a concentration of 2 mg/mL. Strikingly, neither the C_{BOV}- nor the C_{BAC}-AONs showed a cytotoxic effect at this higher concentration, suggesting a role for catalase-sensitive ROS in the cytotoxic effect of the 2.5% TAT-polymersomes. In order to examine their ROS-shielding ability, cells were pulse-treated with the indicated concentration of polymersomes for 1 h followed by washing and a 24 h challenge with or without 5 mM exogenous H_2O_2 (Figure 5b). Crystal violet analysis confirmed that under these conditions both AONs can fully protect against H_2O_2 cytotoxicity with the C_{BAC}-AONs being 10–15 times more potent than C_{BOV}-AONs (EC50 values of 10.6 (SD = 0.45) and 166.6 (SD = 58.8) μg/mL, respectively). This difference in dose-dependence mirrors is determined in vitro (Figure S14), and demonstrates the robustness of this platform where function in vitro is directly translated in cellulo. Next, we used the chloromethyl (CM) variant of the ROS-reactive fluorescent probe 2′,7′-dichlorodihydrofluorescein diacetate (CM-H_2DCFDA) to demonstrate the H_2O_2 detoxifying effect of the AONs. CM-H_2DCFDA is intracellularly trapped as nonfluorescent covalently coupled CM-H_2DCF, and exogenous H_2O_2 induces its oxidation to fluorescent CM-DCF, a measure of intracellular ROS.[79] Cells treated with 0.4 mg/mL AONs for 24 h, and subsequently loaded with CM-H_2DCF,

were challenged for 5 min with 0.5 mM exogenous H_2O_2 and subsequently analyzed by flow cytometry. The average fluorescence intensity of at least 10 000 counted cells was measured showing that exogenous H_2O_2 significantly increased intracellular ROS in both nontreated cells and cells treated with empty 2.5% TAT-polymersomes, an effect that was completely reversed by the C_{BAC}-AONs and partly by the C_{BOV}-AONs (Figure 5c). In accordance with the results of the cytotoxicity study, 2.5% TAT-polymersomes alone did not cause any increase in CM-H_2DCF oxidation at the concentration used.

ROS Shielding by AONs in Primary Skin Fibroblasts from Patients with Isolated Mitochondrial Complex I Deficiency. Primary skin fibroblasts from patients with isolated mitochondrial complex I deficiency show an increased oxidation of ROS probes, suggesting a misbalance between ROS production and scavenging. Using primary skin fibroblasts from a healthy individual (C5120) and a patient with a mutation in the structural NDUFS7 subunit of CI (S7-5175), we assessed the ability of the C_{BAC}-AONs to protect against H_2O_2 cytotoxicity. Evaluation of the CM-DCF signal after 24 h of treatment with 0.4 mg/mL of AONs (followed by a 5 min challenge with 0.5 mM exogenous H_2O_2) showed that the H_2O_2-induced increase in fluorescence was virtually completely blunted (Figure 6a). Both in nontreated cells and in cells treated with empty 2.5% TAT-polymersomes the H_2O_2-induced increase in CM-DCF fluorescence was significantly higher in patient cells, suggesting a reduced capacity to detoxify this ROS. Critically, this difference was no longer observed following AON treatment, demonstrating a clear improvement of the ROS detoxifying capability. To assess the effect of AONs on H_2O_2 cytotoxicity, fibroblasts were pulse-treated with polymersomes for 1 h followed by their removal and a chase period of 4 h prior to a 24 h challenge with or without 0.1 mM exogenous H_2O_2. Subsequent crystal violet analysis demonstrated the dose-dependence of the effect of C_{BAC}-AONs in both healthy and patient fibroblasts (Figure 6b,c). In both cases complete prevention was obtained at an AON concentration of 0.3 mg/mL. In comparison, free C_{BAC} at an equivalent concentration of 0.042 mg/mL had only a

minor, if any, preventive effect in both control and patient cells (Figure S16). These results are in agreement with the above conclusion that 2.5% TAT-polymersomes possess strong uptake-facilitating properties and, in addition, demonstrate that the activity of encapsulated C_{BAC} is preserved for at least 28 h in the endolysosomal system.

CONCLUSION

In summary, we have shown the engineering of a biodegradable, intrinsically permeable nanoreactor, comprising enzyme-loaded PEG−PCLgTMC polymersomes, which, for the first time, demonstrate a therapeutic effect in primary human cells. These autonomous nanoreactors, when modified with cell-penetrating peptides, were capable of cellular integration, delivering macromolecular cargo via the endolysosomal system. To demonstrate functional engagement of these synthetic organelles within the cell, catalase-loaded, antioxidant nanoreactors (AONs) were employed to achieve shielding from reactive oxygen species in both HEK293 cells and primary human fibroblasts. In robust biochemical assays, we demonstrated that AONs successfully protected the cells from exogenous H_2O_2-induced cell death and further demonstrated H_2O_2 detoxification using a fluorogenic ROS probe. The protection of particularly sensitive human fibroblasts puts the application of synthetic organelles in a therapeutically relevant context using primary tissue, with significant evidence of the function *in vitro*. This work, therefore, constitutes the development of a realizable therapeutic technology, facilitated by the synergy between materials engineering and biochemical analysis.

METHODS AND MATERIALS

All chemicals and enzymes were used as received unless otherwise stated. For the synthesis of the block copolymers, monodisperse heterobifunctional (methoxy-hydroxyl and methoxy-carboxyl) PEG macroinitiators were purchased from Creative PEG Works. Trimethylene carbonate was purchased from Acros Organics. Ultrapure Milli-Q water, obtained from a Labconco Water Pro PS purification system (18.2 MΩ), was used for the polymersome preparation. Dialysis membrane from spectrum laboratories (1000 kDa MWCO) and Superose 6 (GE Healthcare) SEC column were used for purification. All enzymes were supplied by Sigma-Aldrich: catalase from bovine liver (E.C. 232-577-1, E3289), catalase from *Corynebacterium glutamicum* (E.C. 1.11.1.6, 02071), glucose oxidase from *Aspergillus niger* (E.C. 232-601-0, G7141), and horseradish peroxidase (E.C. 232-668-6, P6782). All chemicals, unless otherwise stated, were supplied by Sigma-Aldrich.

Synthesis of Poly(ethylene glycol)-*block*-Poly-(caprolactone-*gradient*-trimethylene carbonate). This polymer was synthesized using ring-opening polymerization and MSA as a catalyst. The polymer chain length and the dispersity were determined by ¹H NMR and GPC. The detailed synthetic procedure is described in the Supporting Information.

General Procedure for Polymersome Formation and Encapsulation of Enzymes. In a 5 mL vial, 20 μL of PEG−PCLgTMC block copolymer (10% in PEG 350 w/w) was added. A magnetic stirring bar was added, and a thin film of the polymer solution was created by slow stirring. Subsequently, 80 μL of aqueous solution was directly added, followed by continuous stirring for 5 min. Polymersomes were sub-

sequently diluted until the desired concentration was reached. In order to encapsulate enzymes, polymersomes were prepared by addition of 80 μL of aqueous solution containing the desired concentration of enzyme(s) (typically 5−10 mg/mL) for encapsulation.

Cell Culture. HEK293T cells were grown as a monolayer in DMEM with GlutaMax, high glucose, and pyruvate (31966 GIBCO, Life Technologies Invitrogen, Breda, The Netherlands) supplemented with 10% (v/v) fetal calf serum (FCS) (GIBCO, Life Technologies Invitrogen) and 100 IU/mL penicillin/streptomycin (15140122 Life Technologies Invitrogen) in a humidified atmosphere of 95% air, 5% CO_2 at 37 °C. Assay medium for HEK293T cells was without glucose, glutamine, phenol red, and sodium pyruvate (A14430-01, GIBCO, Life Technologies), supplied with 10% FCS, 100 IU/mL penicillin/streptomycin, 2 mM L-glutamine (25030-024, Gibco, Life Technologies), 5 mM D-glucose (8769 GIBCO, Life Technologies), and 10 mM HEPES (15630056, Gibco, Life Technologies). Primary human skin fibroblasts were obtained following informed parental consent and according to the relevant Institutional Review Boards from skin biopsies of one healthy subject (C5120) and one patient in whom an isolated complex I deficiency was confirmed in both muscle tissue and cultured fibroblasts (S7-5175). Fibroblasts were grown in medium 199 (M-199) with Earle's salts, L-glutamine, 25 mM HEPES, L-amino acids, and phenol red (12340030 GIBCO, Life Technologies Invitrogen) supplemented with 10% (v/v) FCS and 100 IU/mL penicillin/streptomycin. Assay medium for fibroblasts contained no phenol red (11043-023, GIBCO, Life Technologies Invitrogen).

Confocal Microscopy for Visualizing Uptake in a Cell Monolayer. Two days prior to imaging, HEK293T cells were seeded in complete medium at 40 000 cells/well on an 8-well cover-glass slide (155411, Nunc Lab-Tek Chamber slide 1.0 Borosilicate cover-glass, Nunc, Wiesbaden, Germany). One day before imaging, the medium was replaced by complete medium containing the appropriate concentration of polymersomes. After incubation, the medium including polymersomes was removed, and the cells were washed three times with PBS and imaged in assay medium. Colocalization markers CellMask green (C37608, Life Technologies Invitrogen) and CellMask deep red (C10046, Life Technologies Invitrogen) were used to stain the plasma membrane. Cells were incubated with the 1× working solution (provided solution is 1000×) for 3 min, washed three times with PBS, and imaged within 10 min in assay medium.

Imaging was performed with a TCS SP5 confocal microscope (Leica Microsystems, Mannheim, Germany) equipped with an HCX PL APO 63× N.A. 1.2 water immersion objective. Cells were maintained at 37 °C on a temperature-controlled microscope stage. The polymersomes labeled with NBDand CellMask green were excited by an argon laser at 488 nm, and emission was collected between 500 and 550 nm. Polymersomes including BSA-Alexa647 and CellMask deep red were excited with a 633 nm HeNe laser, and emission was collected between 655 and 750 nm. Both green and red fluorescent labels were excited sequentially. Images were analyzed with Image Pro Plus 6.1 (Media Cybernetics, Rockville, MD) and FIJI software (http://fiji.sc/).

Confocal Microscopy for Visualizing Cellular Trafficking in a Cell Monolayer. Two days prior to imaging, HEK293T cells were seeded in complete medium at 40 000 cells/well on an 8-well cover-glass slide (155411, Nunc Lab-

Tek Chamber slide 1.0 Borosilicate cover-glass, Nunc, Wiesbaden, Germany). One day before imaging, the medium was replaced by complete medium containing the appropriate concentration of polymersomes. After incubation of 1 h, the medium including polymersomes was removed, and the cells were washed two times with PBS and for 24 h incubated with complete medium in a humidified atmosphere of 95% air, 5% CO_2 at 37 °C.

To stain the lysosomes, the cells were incubated with 75 nM LysoTracker green DND-26 (Thermo Fisher Scientific) for 1 h in a humidified atmosphere of 95% air, 5% CO_2 at 37 °C. After removal of staining, the cells were imaged in assay medium. Imaging was performed with a TCS SP8 microscope (Leica Microsystems, Mannheim, Germany) equipped with an HCX PL APO 63× N.A. 1.2. water immersion objective. Cells were maintained at 37 °C on a temperature-controlled microscope stage. LysoTracker green was excited by an argon laser at 488 nm, and emission was collected between 500 and 550 nm. Simultaneously, BSA-Alexa647 was excited with a white light laser at 647 nm, and emission was collected between 655 and 750 nm. Both emission signals were simultaneously recorded with avalanche photodiode/photomultiplier tubes hybrid detectors (HyD, Leica).

Images were analyzed with Image Pro Plus 6.1 (Media Cybernetics, Rockville, MD) and FIJI software (http://fiji.sc/).

Flow Cytometry for Visualizing Uptake of Polymersomes in a Cell Monolayer. HEK293T cells were seeded in 24-well plates (Sarstedt, Numbrecht, Germany) at 80 000 cells/well 2 days prior to measurement. Cells were incubated with the indicated concentration of polymersomes for 24 h. After incubation, the cells were washed 3× with PBS and detached by trypsinisation for 2−3 min, spun down, and resuspended in assay medium. The fluorescent signal of the polymersomes was measured using a FACSCalibur flow cytometer (BD BioSciences, Erembodegem, Belgium), and subsequently data were analyzed with FlowJo software. The cells were gated on the live population by forward and side scatter, and 10 000 cells were counted to determine cellular uptake by measure of mean cellular fluorescence in the FL-I channel.

Flow Cytometry for Measuring ROS Levels. HEK293T cells were seeded in 24-well plates (Sarstedt, Numbrecht, Germany) at 80 000 cells/well and fibroblasts 40 000 cells/well, 2 days prior to measurement. Cells were incubated with the indicated concentration of polymersomes for 24 h. After incubation, the cells were washed 2× with PBS and stained with 5 μM CM-H_2DCFDA (C6827, Invitrogen) in assay medium for 30 min in a humidified atmosphere of 95% air, 5% CO_2 at 37 °C. The staining was aspirated, and subsequently 500 μM H_2O_2 (Scharlau, 30% w/w) in assay medium was added for 5 min in a humidified atmosphere of 95% air, 5% CO_2 at 37 °C. Next, cells were detached by trypsinisation for 2−3 min, spun down, and resuspended in 100 μL of assay medium. The fluorescent signal of H_2DCF was measured using a FACSCalibur flow cytometer (BD BioSciences, Erembodegem, Belgium), and subsequently data were analyzed with FlowJo software. The cells were gated on the live population by forward and side scatter, and 10 000 cells were counted to determine cellular uptake by measure of mean cellular fluorescence in the FL-I channel.

Crystal Violet Assay. Cells were seeded in 24-well plates and subjected to the various treatments (e.g., dose-dependency

polymersomes, H_2O_2). Next, the cells were washed with PBS and incubated for 10 min at room temperature (RT) in a staining solution consisting of 0.5% (w/v) crystal violet solution, 30% (v/v) ethanol, and 3% (v/v) formaldehyde. After staining, plates are rinsed with water followed by addition of a 1% (w/v) SDS solution for 30 min on an orbital shaker. The amount of resolubilized crystal violet can be used as a readout of relative cell numbers by absorbance measurements (550 nm) using a microplate spectrophotometer (Benchmark Plus, Biorad, The Netherlands).[80]

Statistical Analysis. The number of independent experiments is marked by n, each experiment performed in duplicate. Average values are represented as mean ± SD. Values were tested for significance using the two-way analysis of variance (ANOVA) at 95% confidence level ($p < 0.05$), followed by Tukey's multiple comparisons test (Graph Pad Prism software, version 6), unless stated otherwise. Significant differences are indicated by $*P < 0.05$, $**P < 0.01$, $***P < 0.001$, $****P < 0.0001$.

No unexpected or unusually high safety hazards were encountered during this research.

■ ASSOCIATED CONTENT

ⓢ Supporting Information

The Supporting Information is available free of charge on the ACS Publications website at DOI: 10.1021/acscentsci.8b00336.

Characterization of polymersomes and their assembly using different direct hydration formulations, cellular uptake, subcellular distribution studies, and characterization of catalase-loaded AONs (PDF)

■ AUTHOR INFORMATION

Corresponding Authors
*E-mail: P.Willems@ncmls.ru.nl.
*E-mail: d.s.williams@swansea.ac.uk.
*E-mail: j.c.m.v.hest@tue.nl.

ORCID ⓞ
Loai K. E. A. Abdelmohsen: 0000-0002-0094-1893
Daniela A. Wilson: 0000-0002-8796-2274
Roland Brock: 0000-0003-1395-6127
David S. Williams: 0000-0002-8209-6899
Jan C.M. van Hest: 0000-0001-7973-2404

Author Contributions
#L.M.P.E.v.O. and L.K.E.A.A. contributed equally to this research

Notes
The authors declare the following competing financial interest(s): This research was carried out in a collaborative project with Khondrion BV (a Radboud University Medical Centre spin-off biotech company). J.A.M.S. is the founding CEO of Khondrion BV. P.H.G.M.W. and W.J.H.K. are scientific advisors for Khondrion BV. W.J.H.K. is also a scientific advisor of Mitoconix Bio Ltd. (Ness Ziona, Israel).

■ REFERENCES

(1) Buddingh', B. C.; van Hest, J. C. M. Artificial Cells: Synthetic Compartments with Life-like Functionality and Adaptivity. *Acc. Chem. Res.* **2017**, *50*, 769−777.

(2) York-Duran, M. J.; Godoy-Gallardo, M.; Labay, C.; Urquhart, A. J.; Andresen, T. L.; Hosta-Rigau, L. Recent advances in compartmentalized synthetic architectures as drug carriers, cell mimics and artificial organelles. *Colloids Surf., B* **2017**, *152*, 199−213.

(3) Balasubramanian, V.; Herranz-Blanco, B.; Almeida, P. V.; Hirvonen, J.; Santos, H. A. Multifaceted polymersome platforms: Spanning from self-assembly to drug delivery and protocells. *Prog. Polym. Sci.* **2016**, *60*, 51−85.

(4) Peters, R. J. R. W.; Louzao, I.; van Hest, J. C. M. From polymeric nanoreactors to artificial organelles. *Chem. Sci.* **2012**, *3*, 335−342.

(5) Godoy-Gallardo, M.; York-Duran, M. J.; Hosta-Rigau, L. Recent Progress in Micro/Nanoreactors toward the Creation of Artificial Organelles. *Adv. Healthcare Mater.* **2018**, *7*, 1700917.

(6) Gaitzsch, J.; Huang, X.; Voit, B. Engineering Functional Polymer Capsules toward Smart Nanoreactors. *Chem. Rev.* **2016**, *116*, 1053−1093.

(7) Rodríguez-Hernández, J.; Chécot, F.; Gnanou, Y.; Lecommandoux, S. Toward "smart" nano-objects by self-assembly of block copolymers in solution. *Prog. Polym. Sci.* **2005**, *30*, 691−724.

(8) Godoy-Gallardo, M.; Labay, C.; Jansman, M. M. T.; Ek, P. K.; Hosta-Rigau, L. Intracellular Microreactors as Artificial Organelles to Conduct Multiple Enzymatic Reactions Simultaneously. *Adv. Healthcare Mater.* **2017**, *6*, 1601190.

(9) Godoy-Gallardo, M.; Labay, C.; Trikalitis, V. D.; Kempen, P. J.; Larsen, J. B.; Andresen, T. L.; Hosta-Rigau, L. Multicompartment Artificial Organelles Conducting Enzymatic Cascade Reactions inside Cells. *ACS Appl. Mater. Interfaces* **2017**, *9*, 15907−15921.

(10) Tiefenboeck, P.; Kim, J. A.; Trunk, F.; Eicher, T.; Russo, E.; Teijeira, A.; Halin, C.; Leroux, J.-C. Microinjection for the ex Vivo Modification of Cells with Artificial Organelles. *ACS Nano* **2017**, *11*, 7758−7769.

(11) Palivan, C. G.; Goers, R.; Najer, A.; Zhang, X.; Car, A.; Meier, W. Bioinspired polymer vesicles and membranes for biological and medical applications. *Chem. Soc. Rev.* **2016**, *45*, 377−411.

(12) Itel, F.; Schattling, P. S.; Zhang, Y.; Städler, B. Enzymes as key features in therapeutic cell mimicry. *Adv. Drug Delivery Rev.* **2017**, *118*, 94−108.

(13) Jurecka, A.; Tylki-Szymańska, A. Enzyme replacement therapy: lessons learned and emerging questions. *Expert Opin. Orphan Drugs* **2015**, *3*, 293−305.

(14) Ben-Haim, N.; Broz, P.; Marsch, S.; Meier, W.; Hunziker, P. Cell-Specific Integration of Artificial Organelles Based on Functionalized Polymer Vesicles. *Nano Lett.* **2008**, *8*, 1368−1373.

(15) van Dongen, S. F. M.; Verdurmen, W. P. R.; Peters, R. J. R. W.; Nolte, R. J. M.; Brock, R.; van Hest, J. C. M. Cellular Integration of an Enzyme-Loaded Polymersome Nanoreactor. *Angew. Chem., Int. Ed.* **2010**, *49*, 7213−7216.

(16) Tanner, P.; Onaca, O.; Balasubramanian, V.; Meier, W.; Palivan, C. G. Enzymatic Cascade Reactions inside Polymeric Nanocontainers: A Means to Combat Oxidative Stress. *Chem. - Eur. J.* **2011**, *17*, 4552−4560.

(17) Liu, G.-Y.; Chen, C.-J.; Ji, J. Biocompatible and biodegradable polymersomes as delivery vehicles in biomedical applications. *Soft Matter* **2012**, *8*, 8811.

(18) Tanner, P.; Balasubramanian, V.; Palivan, C. G. Aiding Nature's Organelles: Artificial Peroxisomes Play Their Role. *Nano Lett.* **2013**, *13*, 2875−2883.

(19) Thingholm, B.; Schattling, P.; Zhang, Y.; Städler, B. Subcompartmentalized Nanoreactors as Artificial Organelle with Intracellular Activity. *Small* **2016**, *12*, 1806−1814.

(20) Kartha, S.; Yan, L.; Weisshaar, C. L.; Ita, M. E.; Shuvaev, V. V.; Muzykantov, V. R.; Tsourkas, A.; Winkelstein, B. A.; Cheng, Z. Superoxide Dismutase-Loaded Porous Polymersomes as Highly Efficient Antioxidants for Treating Neuropathic Pain. *Adv. Healthcare Mater.* **2017**, *6*, 1700500.

(21) Anraku, Y.; Kishimura, A.; Kamiya, M.; Tanaka, S.; Nomoto, T.; Toh, K.; Matsumoto, Y.; Fukushima, S.; Sueyoshi, D.; Kano, M. R.; Urano, Y.; Nishiyama, N.; Kataoka, K. Systemically Injectable Enzyme-Loaded Polyion Complex Vesicles as In Vivo Nanoreactors Functioning in Tumors. *Angew. Chem., Int. Ed.* **2016**, *55*, 560−565.

(22) Baumann, P.; Spulber, M.; Fischer, O.; Car, A.; Meier, W. Investigation of Horseradish Peroxidase Kinetics in an "Organelle-Like" Environment. *Small* **2017**, *13*, 1603943.

(23) Messager, L.; Burns, J. R.; Kim, J.; Cecchin, D.; Hindley, J.; Pyne, A. L. B.; Gaitzsch, J.; Battaglia, G.; Howorka, S. Biomimetic Hybrid Nanocontainers with Selective Permeability. *Angew. Chem., Int. Ed.* **2016**, *55*, 11106−11109.

(24) Lomora, M.; Garni, M.; Itel, F.; Tanner, P.; Spulber, M.; Palivan, C. G. Polymersomes with engineered ion selective permeability as stimuli-responsive nanocompartments with preserved architecture. *Biomaterials* **2015**, *53*, 406−414.

(25) Gräfe, D.; Gaitzsch, J.; Appelhans, D.; Voit, B. Cross-linked polymersomes as nanoreactors for controlled and stabilized single and cascade enzymatic reactions. *Nanoscale* **2014**, *6*, 10752−10761.

(26) Langowska, K.; Palivan, C. G.; Meier, W. Polymer nanoreactors shown to produce and release antibiotics locally. *Chem. Commun.* **2013**, *49*, 128−130.

(27) Gaitzsch, J.; Appelhans, D.; Wang, L.; Battaglia, G.; Voit, B. Synthetic Bio-nanoreactor: Mechanical and Chemical Control of Polymersome Membrane Permeability. *Angew. Chem., Int. Ed.* **2012**, *51*, 4448−4451.

(28) Balasubramanian, V.; Onaca, O.; Ezhevskaya, M.; Van Doorslaer, S.; Sivasankaran, B.; Palivan, C. G. A surprising system: polymeric nanoreactors containing a mimic with dual-enzyme activity. *Soft Matter* **2011**, *7*, 5595.

(29) Onaca, O.; Hughes, D. W.; Balasubramanian, V.; Grzelakowski, M.; Meier, W.; Palivan, C. G. SOD Antioxidant Nanoreactors: Influence of Block Copolymer Composition on the Nanoreactor Efficiency. *Macromol. Biosci.* **2010**, *10*, 531−538.

(30) Nardin, C.; Thoeni, S.; Widmer, J.; Winterhalter, M.; Meier, W. Nanoreactors based on (polymerized) ABA-triblock copolymer vesicles. *Chem. Commun.* **2000**, *0*, 1433−1434.

(31) Garni, M.; Thamboo, S.; Schoenenberger, C.-A.; Palivan, C. G. Biopores/membrane proteins in synthetic polymer membranes. *Biochim. Biophys. Acta, Biomembr.* **2016**, *1859*, 619−638.

(32) Abdelmohsen, L. K. E. A.; Nijemeisland, M.; Pawar, G. M.; Janssen, G. J. A.; Nolte, R. J. M.; Van Hest, J. C. M.; Wilson, D. A. Dynamic Loading and Unloading of Proteins in Polymeric Stomatocytes: Formation of an Enzyme-Loaded Supramolecular Nanomotor. *ACS Nano* **2016**, *10*, 2652−2660.

(33) Nijemeisland, M.; Abdelmohsen, L. K. E. A.; Huck, W. T. S.; Wilson, D. A.; van Hest, J. C. M. A Compartmentalized Out-of-Equilibrium Enzymatic Reaction Network for Sustained Autonomous Movement. *ACS Cent. Sci.* **2016**, *2*, 843−849.

(34) Vriezema, D. M.; Garcia, P. M. L.; Sancho Oltra, N.; Hatzakis, N. S.; Kuiper, S. M.; Nolte, R. J. M.; Rowan, A. E.; Van Hest, J. C. M. Positional assembly of enzymes in polymersome nanoreactors for cascade reactions. *Angew. Chem., Int. Ed.* **2007**, *46*, 7378−7382.

(35) Kuiper, S. M.; Nallani, M.; Vriezema, D. M.; Cornelissen, J. J. L. M.; van Hest, J. C. M.; Nolte, R. J. M.; Rowan, A. E. Enzymes containing porous polymersomes as nano reaction vessels for cascade reactions. *Org. Biomol. Chem.* **2008**, *6*, 4315−4318.

(36) van Dongen, S. F. M.; Nallani, M.; Cornelissen, J. J. L. M.; Nolte, R. J. M.; van Hest, J. C. M. A Three-Enzyme Cascade Reaction through Positional Assembly of Enzymes in a Polymersome Nanoreactor. *Chem. - Eur. J.* **2009**, *15*, 1107−1114.

(37) Louzao, I.; Van Hest, J. C. M. Permeability Effects on the Efficiency of Antioxidant Nanoreactors. *Biomacromolecules* **2013**, *14*, 2364−2372.

(38) Peters, R. J. R. W.; Marguet, M.; Marais, S.; Fraaije, M. W.; van Hest, J. C. M.; Lecommandoux, S. Cascade Reactions in Multi-compartmentalized Polymersomes. *Angew. Chem., Int. Ed.* **2014**, *53*, 146−150.

(39) van Oers, M.; Rutjes, F.; van Hest, J. Cascade reactions in nanoreactors. *Curr. Opin. Biotechnol.* **2014**, *28*, 10−16.

(40) Blackman, L. D.; Varlas, S.; Arno, M. C.; Fayter, A.; Gibson, M. I.; O'Reilly, R. K. Permeable Protein-Loaded Polymersome Cascade Nanoreactors by Polymerization-Induced Self-Assembly. *ACS Macro Lett.* **2017**, *6*, 1263−1267.

(41) Sui, X.; Kujala, P.; Janssen, G.-J.; de Jong, E.; Zuhorn, I. S.; van Hest, J. C. M. Robust formation of biodegradable polymersomes by direct hydration. *Polym. Chem.* **2015**, *6*, 691−696.

(42) O'Neil, C. P.; Suzuki, T.; Demurtas, D.; Finka, A.; Hubbell, J. a. A novel method for the encapsulation of biomolecules into polymersomes via direct hydration. *Langmuir* **2009**, *25*, 9025−9029.

(43) Koopman, W. J. H.; Nijtmans, L. G. J.; Dieteren, C. E. J.; Roestenberg, P.; Valsecchi, F.; Smeitink, J. A. M.; Willems, P. H. G. M. Mammalian Mitochondrial Complex I: Biogenesis, Regulation, and Reactive Oxygen Species Generation. *Antioxid. Redox Signaling* **2010**, *12*, 1431−1470.

(44) Sies, H. Hydrogen peroxide as a central redox signaling molecule in physiological oxidative stress: Oxidative eustress. *Redox Biol.* **2017**, *11*, 613−619.

(45) Sies, H. Oxidative stress: a concept in redox biology and medicine. *Redox Biol.* **2015**, *4*, 180−183.

(46) Gorrini, C.; Harris, I. S.; Mak, T. W. Modulation of oxidative stress as an anticancer strategy. *Nat. Rev. Drug Discovery* **2013**, *12*, 931−947.

(47) Fruehauf, J. P.; Meyskens, F. L. Reactive Oxygen Species: A Breath of Life or Death? *Clin. Cancer Res.* **2007**, *13*, 789−794.

(48) Nogueira, V.; Hay, N. Molecular Pathways: Reactive Oxygen Species Homeostasis in Cancer Cells and Implications for Cancer Therapy. *Clin. Cancer Res.* **2013**, *19*, 4309−4314.

(49) Góth, L.; Nagy, T. Acatalasemia and diabetes mellitus. *Arch. Biochem. Biophys.* **2012**, *525*, 195−200.

(50) Ho, Y.-S.; Xiong, Y.; Ma, W.; Spector, A.; Ho, D. S. Mice Lacking Catalase Develop Normally but Show Differential Sensitivity to Oxidant Tissue Injury. *J. Biol. Chem.* **2004**, *279*, 32804−32812.

(51) Treuting, P. M.; Linford, N. J.; Knoblaugh, S. E.; Emond, M. J.; Morton, J. F.; Martin, G. M.; Rabinovitch, P. S.; Ladiges, W. C. Reduction of age-associated pathology in old mice by overexpression of catalase in mitochondria. *J. Gerontol., Ser A* **2008**, *63*, 813−822.

(52) Dai, D.-F.; Santana, L. F.; Vermulst, M.; Tomazela, D. M.; Emond, M. J.; MacCoss, M. J.; Gollahon, K.; Martin, G. M.; Loeb, L. A.; Ladiges, W. C.; Rabinovitch, P. S. Overexpression of Catalase Targeted to Mitochondria Attenuates Murine Cardiac Aging. *Circulation* **2009**, *119*, 2789−2797.

(53) Olsen, R. H. J.; Johnson, L. A.; Zuloaga, D. G.; Limoli, C. L.; Raber, J. Enhanced hippocampus-dependent memory and reduced anxiety in mice over-expressing human catalase in mitochondria. *J. Neurochem.* **2013**, *125*, 303−313.

(54) Verkaart, S.; Koopman, W. J. H.; Cheek, J.; van Emst-de Vries, S. E.; van den Heuvel, L. W. P. J.; Smeitink, J. A. M.; Willems, P. H. G. M. Mitochondrial and cytosolic thiol redox state are not detectably altered in isolated human NADH:ubiquinone oxidoreductase deficiency. *Biochim. Biophys. Acta, Mol. Basis Dis.* **2007**, *1772*, 1041−1051.

(55) Verkaart, S.; Koopman, W. J. H.; van Emst-de Vries, S. E.; Nijtmans, L. G. J.; van den Heuvel, L. W. P. J.; Smeitink, J. A. M.; Willems, P. H. G. M. Superoxide production is inversely related to complex I activity in inherited complex I deficiency. *Biochim. Biophys. Acta, Mol. Basis Dis.* **2007**, *1772*, 373−381.

(56) Liu, L.; Zhang, K.; Sandoval, H.; Yamamoto, S.; Jaiswal, M.; Sanz, E.; Li, Z.; Hui, J.; Graham, B. H.; Quintana, A.; Bellen, H. J. Glial Lipid Droplets and ROS Induced by Mitochondrial Defects Promote Neurodegeneration. *Cell* **2015**, *160*, 177−190.

(57) Tian, H.; Tang, Z.; Zhuang, X.; Chen, X.; Jing, X. Biodegradable synthetic polymers: Preparation, functionalization and biomedical application. *Prog. Polym. Sci.* **2012**, *37*, 237−280.

(58) Zou, T.; Dembele, F.; Beugnet, A.; Sengmanivong, L.; Trepout, S.; Marco, S.; de Marco, A.; Li, M.-H. Nanobody-functionalized PEG-b-PCL polymersomes and their targeting study. *J. Biotechnol.* **2015**, *214*, 147−155.

(59) Qi, W.; Ghoroghchian, P. P.; Li, G.; Hammer, D. A.; Therien, M. J. Aqueous self-assembly of poly(ethylene oxide)-block-poly(ε-caprolactone) (PEO-b-PCL) copolymers: disparate diblock copolymer compositions give rise to nano- and meso-scale bilayered vesicles. *Nanoscale* **2013**, *5*, 10908−10915.

(60) Li, S.; Meng, F.; Wang, Z.; Zhong, Y.; Zheng, M.; Liu, H.; Zhong, Z. Biodegradable polymersomes with an ionizable membrane: Facile preparation, superior protein loading, and endosomal pH-responsive protein release. *Eur. J. Pharm. Biopharm.* **2012**, *82*, 103−111.

(61) Katz, J. S.; Eisenbrown, K. a.; Johnston, E. D.; Kamat, N. P.; Rawson, J.; Therien, M. J.; Burdick, J. a.; Hammer, D. a. Soft biodegradable polymersomes from caprolactone-derived polymers. *Soft Matter* **2012**, *8*, 10853−10862.

(62) Sanson, C.; Schatz, C.; Le Meins, J.-F.; Brûlet, A.; Soum, A.; Lecommandoux, S. Biocompatible and biodegradable poly-(trimethylene carbonate)-b-poly(L-glutamic acid) polymersomes: size control and stability. *Langmuir* **2010**, *26*, 2751−60.

(63) Adams, D. J.; Kitchen, C.; Adams, S.; Furzeland, S.; Atkins, D.; Schuetz, P.; Fernyhough, C. M.; Tzokova, N.; Ryan, A. J.; Butler, M. F. On the mechanism of formation of vesicles from poly(ethylene oxide)-block-poly(caprolactone) copolymers. *Soft Matter* **2009**, *5*, 3086−3096.

(64) Ahmed, F.; Discher, D. E. Self-porating polymersomes of PEG-PLA and PEG-PCL: hydrolysis-triggered controlled release vesicles. *J. Controlled Release* **2004**, *96*, 37−53.

(65) Meng, F.; Hiemstra, C.; Engbers, G. H. M.; Feijen, J. Biodegradable polymersomes. *Macromolecules* **2003**, *36*, 3004−3006.

(66) Sisson, A. L.; Ekinci, D.; Lendlein, A. The contemporary role of??-caprolactone chemistry to create advanced polymer architectures. *Polymer* **2013**, *54*, 4333−4350.

(67) Couffin, A.; Delcroix, D.; Martín-Vaca, B.; Bourissou, D.; Navarro, C. Mild and efficient preparation of block and gradient copolymers by methanesulfonic acid catalyzed ring-opening polymerization of caprolactone and trimethylene carbonate. *Macromolecules* **2013**, *46*, 4354−4360.

(68) Delcroix, D.; Martín-Vaca, B.; Bourissou, D.; Navarro, C. Ring-Opening Polymerization of Trimethylene Carbonate Catalyzed by Methanesulfonic Acid: Activated Monomer versus Active Chain End Mechanisms. *Macromolecules* **2010**, *43*, 8828−8835.

(69) Küchler, A.; Yoshimoto, M.; Luginbühl, S.; Mavelli, F.; Walde, P. Enzymatic reactions in confined environments. *Nat. Nanotechnol.* **2016**, *11*, 409−420.

(70) Wang, F.; Wang, Y.; Zhang, X.; Zhang, W.; Guo, S.; Jin, F. Recent progress of cell-penetrating peptides as new carriers for intracellular cargo delivery. *J. Controlled Release* **2014**, *174*, 126−136.

(71) Bechara, C.; Sagan, S. Cell-penetrating peptides: 20 years later, where do we stand? *FEBS Lett.* **2013**, *587*, 1693−1702.

(72) Frankel, A. D.; Pabo, C. O. Cellular uptake of the tat protein from human immunodeficiency virus. *Cell* **1988**, *55*, 1189−1193.

(73) Vivès, E.; Brodin, P.; Lebleu, B. A Truncated HIV-1 Tat Protein Basic Domain Rapidly Translocates through the Plasma Membrane and Accumulates in the Cell Nucleus. *J. Biol. Chem.* **1997**, *272*, 16010−16017.

(74) Tunnemann, G. Cargo-dependent mode of uptake and bioavailability of TAT-containing proteins and peptides in living cells. *FASEB J.* **2006**, *20*, 1775−1784.

(75) Selby, L. I.; Cortez-Jugo, C. M.; Such, G. K.; Johnston, A. P. R. Nanoescapology: progress toward understanding the endosomal escape of polymeric nanoparticles. *Wiley Interdiscip. Rev. Nanomedicine Nanobiotechnology* **2017**, *9*, e1452.

(76) Nischan, N.; Herce, H. D.; Natale, F.; Bohlke, N.; Budisa, N.; Cardoso, M. C.; Hackenberger, C. P. R. Covalent Attachment of Cyclic TAT Peptides to GFP Results in Protein Delivery into Live Cells with Immediate Bioavailability. *Angew. Chem., Int. Ed.* **2015**, *54*, 1950−1953.

(77) Massignani, M.; LoPresti, C.; Blanazs, A.; Madsen, J.; Armes, S. P.; Lewis, A. L.; Battaglia, G. Controlling Cellular Uptake by Surface Chemistry, Size, and Surface Topology at the Nanoscale. *Small* **2009**, *S*, 2424−2432.

(78) Williams, D. S.; Pijpers, I. A. B.; Ridolfo, R.; van Hest, J. C. M. Controlling the morphology of copolymeric vectors for next generation nanomedicine. *J. Controlled Release* **2017**, *259*, 29−39.

(79) Koopman, W. J. H.; Verkaart, S.; van Emst-de Vries, S. E.; Grefte, S.; Smeitink, J. A. M.; Willems, P. H. G. M. Simultaneous quantification of oxidative stress and cell spreading using 5-(and-6)-chloromethyl-2′,7′-dichlorofluorescein. *Cytometry, Part A* **2006**, *69A*, 1184−1192.

(80) Śliwka, L.; Wiktorska, K.; Suchocki, P.; Milczarek, M.; Mielczarek, S.; Lubelska, K.; Cierpiał, T.; Łyżwa, P.; Kiełbasiński, P.; Jaromin, A.; Flis, A.; Chilmonczyk, Z. The Comparison of MTT and CVS Assays for the Assessment of Anticancer Agent Interactions. *PLoS One* **2016**, *11*, e0155772.